Structure and Quantification of Edge Sites of WS 2 /Al 2 O 3 Catalysts Coupling IR/CO Spectroscopy and DFT Calculations

Luz Zavala-sanchez, Ibrahim Khalil, Laetitia Oliviero, Jean-François Paul, Françoise Maugé

Structure and quantification of edge sites of WS_2/Al_2O_3 catalysts coupling IR/CO spectroscopy and DFT calculations

Luz Zavala-Sanchez[a], Ibrahim Khalil[a], Laetitia Oliviero[a], Jean-François Paul*[b], Françoise Maugé*[a]

[a] Dr. L. Zavala-Sanchez, Dr. I. Khalil, Dr. L. Oliviero, Dr. F. Maugé,
Normandie Université, ENSICAEN, UNICAEN, CNRS,
Laboratoire Catalyse et Spectrochimie
6, bd du Maréchal Juin, 14050 Caen (France).
E-mail : francoise.mauge@ensicaen.fr
Tel: + 33 (0)2 31 45 28 24

[b] Prof. Dr. J.F. Paul
Université Lille, CNRS, ENSCL, Centrale Lille, UMR 8181-UCCS,
Unité de Catalyse et Chimie du Solide,
Lille F-59000 (France).
E-mail : Jean-Francois.Paul@univ-lille1.fr
Tel: + 33 (0)3 20 33 77 34

KEYWORDS: Hydrotreating catalyst, Tungsten disulfide (WS_2), CO adsorption, IR spectroscopy, density functional theory, morphology.

ABSTRACT

IR spectroscopy of CO adsorption (IR/CO) and Density Functional Theory (DFT) calculations on sulfide W/Al_2O_3 catalyst were investigated for an insight into the sulfide edge sites. Parallel between experimental and theoretical results allow to assign the *v*(CO) bands at 2121 and 2066 cm^{-1} to CO adsorption on M- and S-edge sites of WS_2 phase, respectively.

Through a careful analysis of CO spectra on well-selected W catalysts, the molar attenuation coefficients for CO adsorbed on the two exposed edges could be determined. This allowed the morphology of WS_2 slabs to be calculated. This work shows that increasing the W loading (6-20 wt% W) changes the slab morphology from an almost pure triangle exhibiting mostly M-edge to a truncated triangle.

On W as well as on Mo sulfide catalysts, IR spectroscopy and DFT calculation show that CO adsorption allows to account for M- and S-edge sites, and thus of the morphology of sulfide slabs. It was shown that increasing the W loading shifts the slab morphology from a triangle exposing predominantly M-edge towards a more hexagonal shape. For close to monolayer coverage of alumina, Mo and W sulfide slabs present similar shape i.e. truncated triangle. However, edge sites of WS_2 slabs clearly exhibit greater stability under H_2 atmosphere than Mo sulfided ones.

1. INTRODUCTION

Hydrotreating (HDT) of petroleum fractions is one of the central refining processes to produce clean fuels that meet stringent current ecological requirements. The present challenge is to meet the current requirements for ultra-low sulfur content in fuels by

extracting from heavier oil deposits. Hydrodesulfurization (HDS) is a key process in refineries where transition metal disulfides (TMS) supported on gamma alumina (γ-Al_2O_3) are used for HDT processes. Among the different metals, Mo or W disulfides with Co or Ni metals as promoters have shown the most promising results in this field. The CoMo and NiMo/Al_2O_3 catalysts have been extensively studied, meanwhile NiW catalysts have remained less investigated.[1] The importance of NiW/Al_2O_3 sulfide catalysts is given by their excellent performance in hydrogenation reactions for deep HDS, providing a high potential for the conversion of alkyl-dibenzothiophenes (alkyl-DBTs).[2,3] HDS catalysts have been the subject of numerous characterization studies,[4] and presently there is a general agreement that the sulfide phase MoS_2 (WS_2) presents a lamellar structure, formed by layers of MS_2 (M=W, Mo). The 2D morphology of these layers, their average stacking (~2 to 4) and their average size (~3 to 6 nm) depends on the sulfidation conditions, the metal loading among other parameters. Many correlations between the structure and the activity of these systems link the catalytic reaction to the sites along the edges of the individual layers MS_2. At this location, the promoter atoms are also found in the so-called CoMoS type structures (NiMoS, CoWS and NiWS).[5] The MS_2 slabs expose principally two types of edges: the metal terminated edge (M-edge) and the sulfur terminated edge (S-edge). Studies also indicates that M-edge and S-edge sites have different intrinsic activities in HDS reactions, S-edge being more active and more favorable for the promotion and the formation of the promoted phase.[6]

An informative way to characterize sulfide sites on these catalysts is the low temperature CO adsorption followed by IR spectroscopy (IR/CO). In addition to the detection of the sulfide sites, this characterization offers the advantage of quantifying

their concentration by means of the molar attenuation coefficient, and thus gives access to sulfide phase dispersion and intrinsic activity of the sulfide sites (ref).[7] It should be mentioned that several ν(CO) bands characterized the sulfide sites, even on unpromoted catalysts. Unequivocal attribution of the CO adsorption bands to sites of specific sulfide structures cannot be achieved by IR spectroscopy alone. The continuous development of modeling techniques as the Density Functional Theory (DFT) allows defining realistic surfaces models. The modeling of the stable sulfide surfaces according to the sulfide atmosphere is a powerful approach to obtain a description of the various CO adsorption sites.[8,9] Hence for MoS_2, Travert et al. demonstrated that the coupling of techniques as IR/CO and DFT permitted to attribute the main ν(CO) bands to M-edge sites and to S-edge sites as well as to show that these sulfide sites can be modified by post-treatments with hydrogen.[10,11] Further, determination of the molar attenuation coefficients of ν(CO) band characteristics of the M-edge and S-edge sites allowed quantification of these two edges and thus assessment of the morphology of MoS_2 slabs.[12] It was thus possible to demonstrate that the MoS_2 morphology (expressed by S_{edge}/M_{edge} ratio) varies with the preparation parameters (metal loading, chelating agent addition, support nature) [7,13–15] and the sulfidation conditions. [13,16] Recent observations of the sulfide catalysts by STEM HAADF confirmed the morphology of the MoS_2 slabs deduced from the spectroscopic analysis[17]. These knowledge allows a controlled design of the MoS_2-based slabs from a slightly truncated to heavily truncated triangle sulfided slab morphology.

In comparison with Mo catalysts, W based ones are less documented in literature.[18] Although a considerable amount of research has been made on their

activity, selectivity and in general catalytic properties of the W catalysts, an accurate description of the active sites is still lacking.[13,19,20] So far the available CO spectra representing W-based catalyst are rather limited, and no reports were established on the assignment of their specific IR/CO bands, neither on the quantification of these edge sites. Hence, this paper presents an insight into the sulfided W/Al_2O_3 system characterized through IR spectroscopy and DFT calculation. We first perform the IR/CO adsorption experiments over W/Al_2O_3 catalyst, later the modeling of the WS_2 (1 0 0) stable surfaces and the calculation of the stretching frequencies of CO adsorbed on these surfaces. The parallel between experimental and theoretical results allows assigning the bands at 2121 and ~2066 cm^{-1} to CO adsorbed on M- and S-edge sites, respectively. In a further step, the molar attenuation coefficient of these bands was determined that allows accounting for the effect of W loading on the WS_2 slab morphology.

2. EXPERIMENTAL SECTION

2.1. Catalyst preparation.

The studied materials consisted in a series of non-promoted W/Al_2O_3 catalyst prepared by a one-step pore volume impregnation method with variable W loading (6, 9, 12, 16 and 20 W wt. %), 20 W wt. % corresponding to 3.3 atoms·nm^{-2}, e.g. a submonolayer of W atoms (oxidic form). The catalysts were impregnated with an aqueous solution of appropriate amounts of hydrated ammonium metatungstate ($(NH_4)_6H_2W_{12}O_{40}\cdot H_2O$ SIGMA-ALDRICH) on commercial γ-Al_2O_3 support (SASOL extrudates, specific surface area of 252 $m^2\cdot g^{-1}$ and pore volume of 0.82 $ml\cdot g^{-1}$, precalcined in air flow at 723 K for 4

h. After impregnation, the materials were left for maturation at room temperature for 2 h and subsequently the complete catalyst series was thermally treated at 383 K for 16 h inside a rotatory furnace under air 100 ml·min^{-1} flow and a heating rate of 3 K·min^{-1}. Hereinafter, the W/Al_2O_3 catalysts are denoted as X_W/Al_2O_3 where X refers to the W wt. % loading in the catalysts.

2.2. Low temperature CO adsorption followed by IR spectroscopy characterization (IR/CO).

The WS_2 edge sites of these catalysts were characterized by low-temperature (~100 K) CO adsorption followed by IR spectroscopy (IR/CO). CO adsorption was performed at low temperature to avoid any reaction with the catalysts surface and to strengthen the interaction with the weakest adsorption sites of the catalyst surface. The oxide catalyst was grounded and pressed into self-supported wafer (ca. 10 mg, precisely weighted, for a 2.01 cm^2 disc) and placed into a quartz IR cell with CaF_2 windows. After *in situ* sulfidation under 10% H_2S/H_2 with a flow rate of 30 ml·min^{-1} for 2 h at 673 K (sulfidation starting from room temperature with a heating rate of 3 K.min^{-1}), the cell was flushed with Ar for 10 min and evacuated down to P<1·10^{-4} Pa maintaining the 673 K temperature during 1 h. Finally, the sample was cooled down to room temperature and further down to 100 K under vacuum. CO adsorption experiments were performed introducing small calibrated CO doses and then an equilibrium pressure of 133 Pa. Note that it was ensured that this protocol of sulfidation yields to catalysts with a WS_2 amount that is comprised between 92 and 100% whatever the W loading.

After the sulfidation following the previous procedure, pure hydrogen post-treatment was performed on the 20_W/Al_2O_3 catalyst. In such a case, the sulfide catalyst was *in*

situ reduced under pure H_2 with a flow rate of 50 ml·min^{-1} at 673 K for 2 h. After the aforementioned treatment, the sample was flushed under Ar flow for 10 minutes and the temperature was cooled down under high vacuum (P = 9.7 × 10^{-5} Pa residual pressure) to room temperature and then to 100 K to perform CO adsorption.

FTIR spectra were recorded with 256 scans and a resolution of 4 cm^{-1} using Nicolet Nexus FTIR spectrometer equipped with a MCT detector (FTIR= Fourier Transform Infrared; MCT=Mercury-Cadmium-Tellurium). All spectra were normalized to a disc of 5 mg·cm^{-2}. The bands of the adsorbed CO species were obtained by subtracting the spectra recorded after CO adsorption minus before. All experiments were duplicated, with a maximum error of 5%. The band areas of the different v(CO) components that characterize the WS_2 can be obtained by careful spectrum decomposition. In this work, the decomposition was done with Peakfit V4.12 software using the "Autofit peak III decomposition Method". Before the decomposition, second derivative of the spectra was performed to determine the number of bands. For the decomposition, the center and full width at half height (FWHH) of each band are allowed to vary in a small range (± 3 cm^{-1}).

2.3. Computational techniques.

2.3.1. Method description: computational parameters.

The density functional theory (DFT) calculations were carried out with the Vienna Ab initio Simulation Package (VASP) software.[21,22] The energy is calculated using the non-local functional generalized gradient corrections (GGA) approximation as parameterized by Perdew et al.[23,24] The wave function is expanded in a plane wave basis set, and the

electron–ion interactions are defined using the Projector Augmented Plane Wave (PAW) method.[25] In order to compute reliable adsorption energies, Van der Waals forces were considered in the calculations. The Perdew-Burke-Ernzerhof (PBE) functional was employed with 0.1 eV Gaussian smearing.[26] It has been shown that PBE gives good results in ionic systems if the Van der Waals interactions are considered.[27] The solution of the Kohn–Sham equation was improved self-consistently until a difference lower than 10^{-5} eV was obtained between successive iterations. The atomic positions were optimized until the forces become less than 0.03 $eV \cdot Å^{-1}$. Test calculations were made by varying cut-off energy from 300 to 600 eV and using the K-points mesh from 3 × 1 × 1 to 5 × 3 × 1 following Monkhorst−Pack[28] schemes to define calculation parameters. From these evaluations, all the bulk and surface calculations were performed with a 550 eV cut-off energy, using a 3 × 3 × 1 K-point mesh for all surface calculations. Using these parameters, the accuracy of the DFT calculation is expected to be better than 0.1 eV for the calculated adsorption energy.

2.3.2. Surface model description.

In the present work we have used a large supercell (12.72 x12.50 x30 $Å^3$) that allows a good description of the WS_2 surface dimensions (see **Figure 1**). This supercell model containing four rows in the x-direction, two layers along the y-direction, and five in the z-direction is appropriate for describing the structural and adsorption properties of the (1 0 0) WS_2 surface. A vacuum layer of 15 Å is located above the WS_2 slab in the z direction in order to avoid interactions between slabs. The three upper W rows and the adsorbed molecules were allowed to relax during the geometry optimization, while the two lower ones were kept fixed at the bulk geometry. The CO vibration frequencies were

calculated by numerical differentiation of the force matrix. The CO stretching vibrational mode being very weakly coupled with the vibration of the surface, only the part of the matrix corresponding to the atoms closest to CO was considered in the diagonalization process of the Hessian matrix.

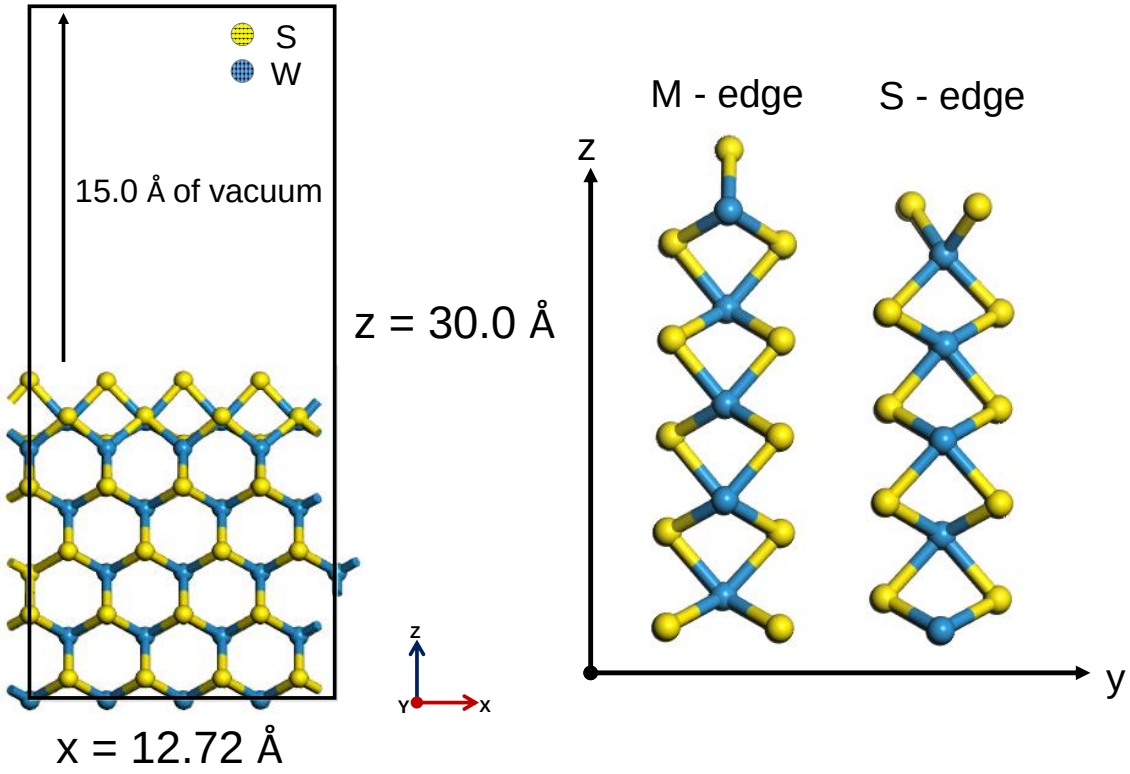

Figure 1. Representation of the supercell used for the calculations, showing the axes. On the left, cell showing the cut WS_2 (1 0 0) surface. Dark circles: W; light circles: S

In order to determine the sulfur coverage of the stable edges, we performed a systematic study varying the sulfur coverage of both edge between 0 and 8, ie starting for the pure W termination to a fully sulfur satured surfaces. We have taken into account the effect of the temperature and pressure by calculation the thermodynamic correction using the classical statistical thermodynamic formalism.[29] At 673 K, the main

contribution to theses correction (c.a. 95%) is due to gas phase molecules (H_2 and H_2S) entropy differences. The surfaces are labeled according to the number of sulfur atoms on the two edges: this is [S atoms $_{M\text{-edge}}$ - S atoms $_{S\text{-edge}}$]. The stability of the surface have been computed using the [4-4] one as reference.

2.4. Determination of molar attenuation coefficients for CO adsorbed on M-edge and S-edge of site WS_2 catalysts.

According to the adapted Beer-Lambert law (Eq. 1) to solid materials, the concentration of sites (*n*, μmol·g^{-1}) on which CO is adsorbed can be calculated using the associated CO molar attenuation coefficient (Ɛ, cm·μmol^{-1}) and the area of ν(CO) band (A, cm^{-1}) normalized to the surface (S, cm^2) and to the mass (m, g) of the catalyst wafer measured after sulfidation:

$$n = \frac{A \times S}{\varepsilon \times m} \qquad (1)$$

The typical CO adsorption experiments on WS_2/Al_2O_3 are performed by adding small CO doses, starting from 9.0x10^{-3} μmol up to 8.64 μmol (cumulative doses) . The Ɛ values can be deduced from the slope of the linear relationship between the area of ν(CO) band (A_{CO}) and the amount of CO introduced onto the sample (n_{CO}) considering that all the introduced doses are adsorbed on the pellet (no residual pressure could be detected in the IR cell). However, the determination of the amount of CO adsorbed on a given site can be very delicate when the CO introduced interacts with several adsorbing sites.

In the present case, we had to determine the molar attenuation coefficient of two ν(CO) bands corresponding to two adsorption sites. It has firstly required the selection

of samples for which analysis of the spectra from the very first doses of CO shows adsorption on only one type of site (Type 1). Thus, the molar attenuation coefficient (ε_1) could be determined using eq. (1).

Then for Type 2 site, the methodology had to be different since none of the spectra whatever the samples show only CO adsorption on this site. Thus, for spectra that present two contributions, the Beer Lambert law can be written as:

$$n_{co} = \frac{A_{CO_1} S}{m\varepsilon_1} + \frac{A_{CO_2} S}{m\varepsilon_2} \qquad (2)$$

The molar attenuation coefficient of CO adsorbed on the second contribution (ε_2) can be determined as follows: after the determination of the area of the two contributions (A_{CO1}, A_{CO2}), the number of CO adsorbed on the site 1 (n_{CO1}) can be calculated from the previously determined ε_1 value. Then, the number of CO adsorbed on the site 2 ($n_{CO1)}$ is determined by subtracting from the total amount of CO introduced n_{CO}, the amount of CO adsorbed on site 1, n_{CO1}. Further, the ε_{CO2} value can be calculated from eq. (2).

The v(CO) band area of the components of CO adsorbed on WS_2 massif was obtained by careful spectrum decomposition using parameters described previously in Section 2.2.

3. RESULTS AND DISCUSSION

3.1. Characterization by low-temperature IR spectroscopy of CO.

3.1.1. IR/CO of sulfided WS_2/Al_2O_3 catalyst.

The IR spectra of CO adsorbed on sulfided 20_W/Al_2O_3 catalyst are presented in **Figure 2**. Four main bands at 2185, 2160, 2121, and 2066 cm^{-1} were detected. The intensity of these bands increases with the amount of CO introduced. The higher wavenumber bands, namely 2185 and 2160 cm^{-1}, are attributed to coordination of CO on Lewis acid sites (Al^{3+}) of the alumina support and CO on hydrogen bonding with the support hydroxyl groups (OH), respectively.[12,30,31] Whereas the bands located at 2121 cm^{-1} and 2066 cm^{-1} are attributed to CO adsorbed on edge sites of the WS_2 slabs. At higher CO uptake appears a shoulder at 2141 cm^{-1}, corresponding to physisorbed CO. The two bands at 2121 cm^{-1} and 2066 cm^{-1} were observed since the very first introduced CO doses and were attributed to CO in interaction with coordinatively unsaturated W sites (CUS) of low oxidation state.[32] Early work of *Duchet*[30] on W/Al_2O_3 catalysts already reported the presence of two bands at 2110 cm^{-1} and 2060 cm^{-1} on sulfided phase, called W_1 and W_2, respectively. On the other hand, *Crepeau* in his work on WS_2/ASA,[33] reported the presence of W_1 and W_2 bands at 2127 cm^{-1} and 2072 cm^{-1}. The difference in the wavenumber between that reported by *Duchet* on WS_2/Al_2O_3 and by *Crepeau* on WS_2/ASA shows that the bands characteristic of the WS_2 phase are also sensitive to the nature of the support.

The inset **Figure 3-A** that reports the spectra normalized to the most intense band, reveals that the band width located at 2121 cm^{-1} (W_1) remains without alteration whatever the amount of CO introduced meanwhile the band at ~ 2066 cm^{-1} shifts and

widens. A closer inspection to the spectra at intermediate CO doses was carried out with the help of the second derivative function (**Figure 3-A**). This analysis points out that at least three components (2075, 2066 and 2051 cm^{-1}) can be distinguished in the W_2 band whereas the W_1 band only comprised one component at 2121 cm^{-1}. This analysis that specifies the maximum of the ν(CO) bands allows to carry out a proper decomposition of the CO spectra.

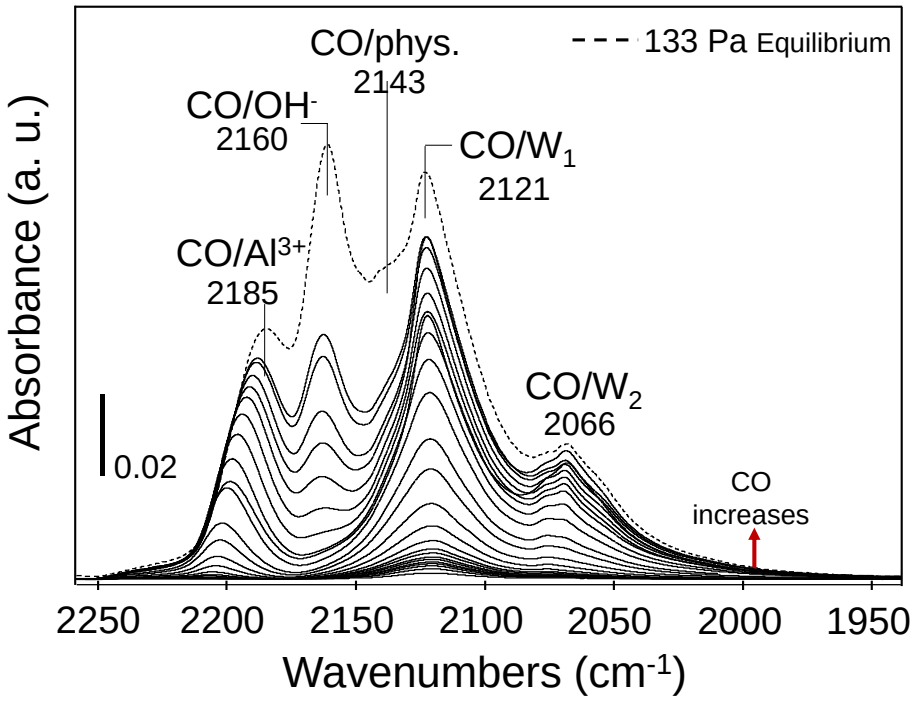

Figure 2. IR spectra of increasing CO doses (up to 133 Pa at equilibrium) adsorbed at 100 K on 20_W/Al_2O_3 catalyst sulfided with 10% H_2S/H_2 at 673 K and 0.1 MPa.

As shown in **Figure 3-B**, on sulfided W/Al_2O_3 catalyst, the obtained IR spectrum was fitted with seven Voigt peaks. The three highest wavenumber peaks used to fit the v(CO) bands were ascribed to: CO coordinated to Lewis acid sites of the alumina support (Al^{+3}): 2186 cm^{-1}, CO in hydrogen bonding with the support hydroxyl groups: 2160 cm^{-1}, and physisorbed CO molecules: 2140 cm^{-1}. Four peaks were generated in

order to fit properly the *v*(CO) bands on WS_2 phase. One peak was used to fit the ν(CO) band on W_1-edge, which is located at 2121 cm^{-1}. Three peaks were employed to fit the v(CO) band on W_2-edge, which are located at 2075, 2066 and 2051 cm^{-1}. This confirms that W_1 band only comprised one single component whereas W_2 band comprised several components whose ratios change with CO doses.

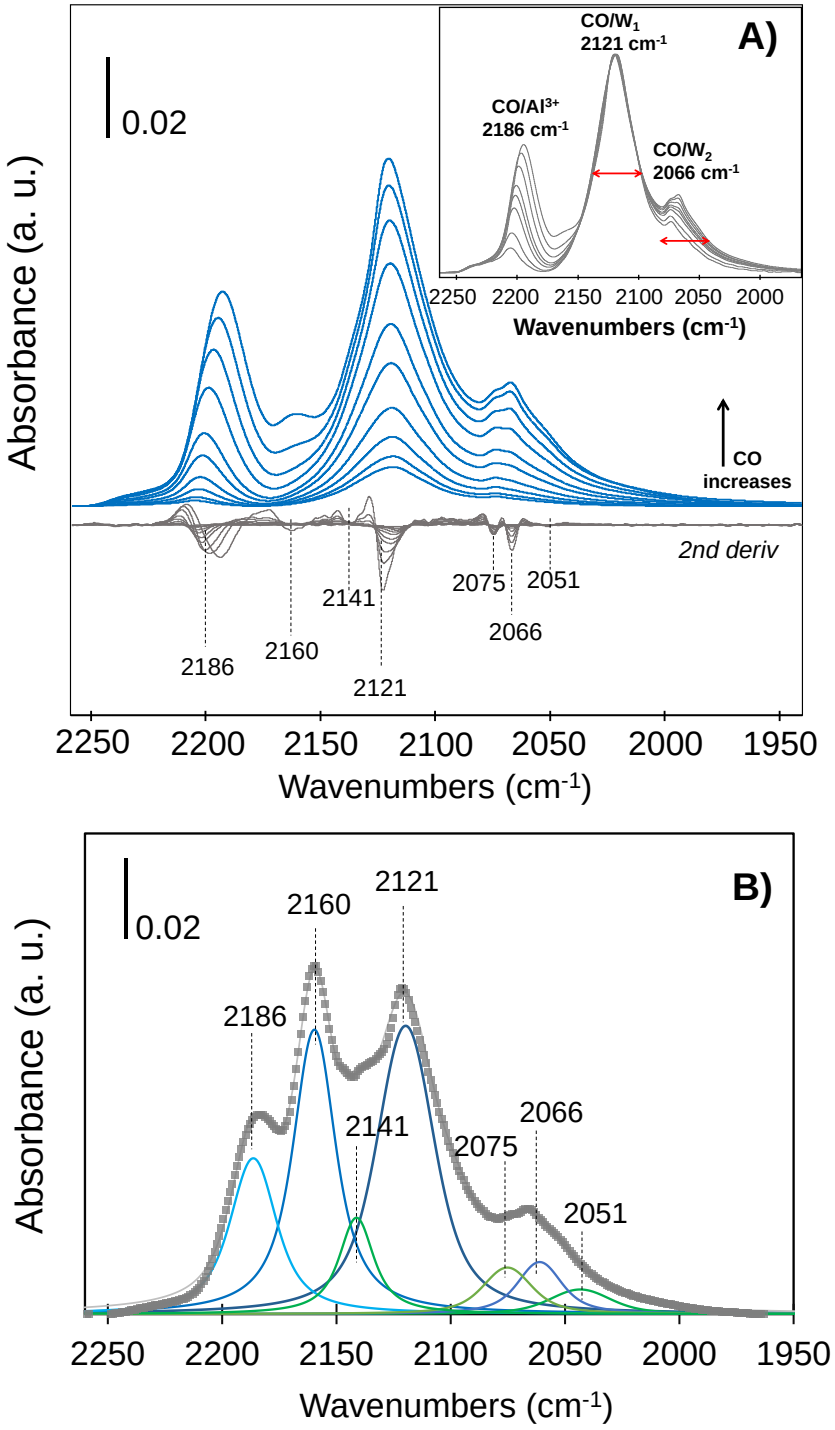

Figure 3. (A) IR spectra of intermediate CO doses adsorbed at 100 K on 20_W/Al_2O_3 catalyst sulfided at 673 K, with their second derivative ; (B) decomposition of the IR spectrum of CO adsorption (P_{CO}=133 Pa at equilibrium).

3.1.2. IR/CO of H_2-treated WS_2/Al_2O_3.

As hydrogen is one of the reactants during the HDS process, its reactivity with HDS catalysts is of great importance.[7,34] Molecular hydrogen can be adsorbed dissociatively on WS_2 edges, leading to the creation of sulfur vacancies by removing sulfur in the form of H_2S and resulting in the WS_2 edges with lower sulfur coverage. The sulfur coverage at the edges of TMS nanoparticles depends on the H_2S/H_2 ratio. Thus, the ease for the creation of sulfur vacancies on the edge sites of the TMS catalyst can be evaluated by comparing the CO uptake before and after the H_2 treatment.[35] In order to investigate the effect of reductive treatment, the sulfided 20_W/Al_2O_3 catalyst was treated under pure H_2 flow for 2 h at 673 K at 1 atm pressure before being characterized by IR/CO. **Figure 4** shows that H_2 post-treatment leads to the increase of intensity of the 2160 and 2186 cm^{-1} bands ascribed to Al^{3+} vacancies and hydroxyl groups of the support: this increase could be explained by evacuation of some adsorbed H_2S during the heating process. As observed in **Figure 4**, the H_2 post-treatment also leads to some increase of the v(CO) intensity in the region corresponding to W_2-edge (2000-2100 cm^{-1}), while the v(CO/W_1-edge) remained practically unchanged. These results indicate that vacancies creation occurs more easily on the W_2-edge and only limited amount of S atoms can be removed from the W_1 edge by H_2 treatment. An inspection in more detail of the three components associated with the W_2-edge reveal that they all increase with a same proportion (Inset **Figure 4**). Nevertheless, it should be underlined that intensity increases of the W_2 bands are small, suggesting that the edges of the sulfided WS_2 slabs are rather stable upon H_2-treatment.

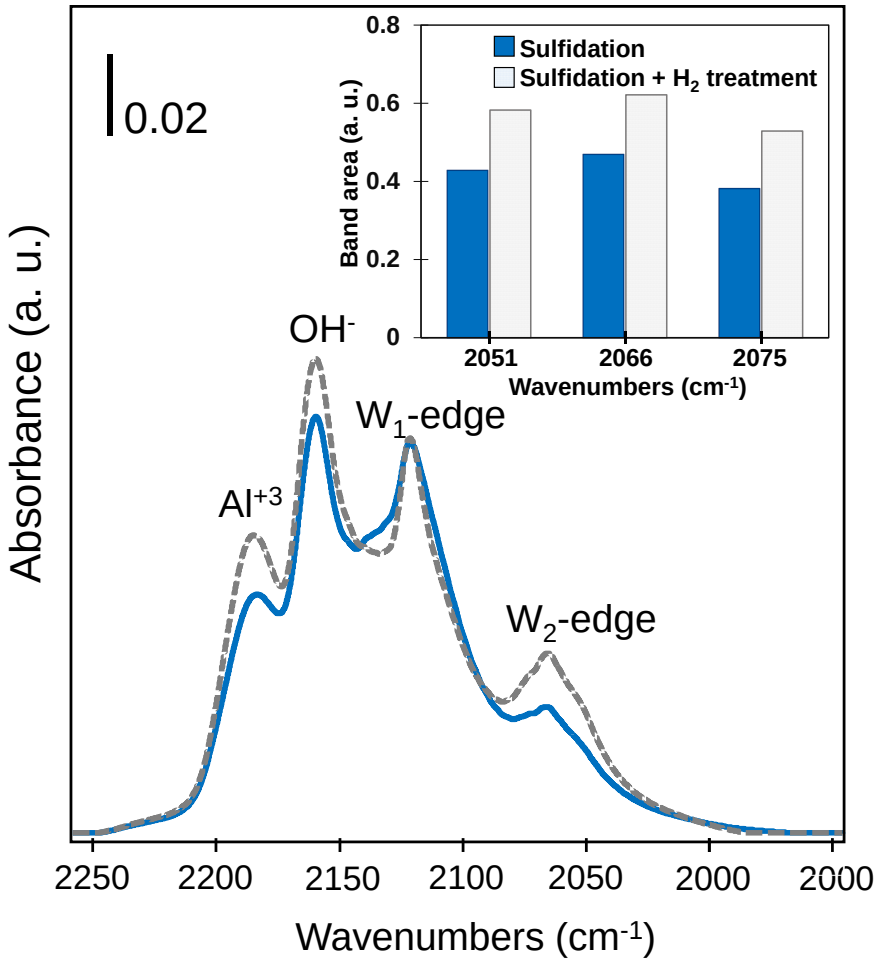

Figure 4. Effect of H_2 treatment at 673 K on CO adsorption (100 K, 133 Pa at equilibrium) on sulfided 20_W/Al_2O_3 catalyst. IR/CO spectrum obtained after sulfidation (continuous line) and after 2 h of H_2 treatment at 673 K (dashed line); Inset: Effect of the H_2 treatment on the area of the IR/CO bands of the three components of W_2 sites.

3.2. DFT calculations

3.2.1. Sulfur coverage and surfaces to study.

By observing the crystallographic structure of the WS_2 slabs, two types of edges are considered, namely, the metallic edge (M-edge) and the sulfur edge (S-edge). It has been shown that the number of sulfur atoms present at the edges of the slabs depends

on the H_2/H_2S molar ratio. Each surface is designated by the number of sulfur atoms exposed on each of the two edges: this is [S atoms $_{M\text{-edge}}$ - S atoms $_{S\text{-edge}}$]. The stability of the surface, compared to the [4-4] one, at 673K, as a function the partial pressure $P(H_2)/P(H_2S)$ logarithm have been computed (**Figure 5**).

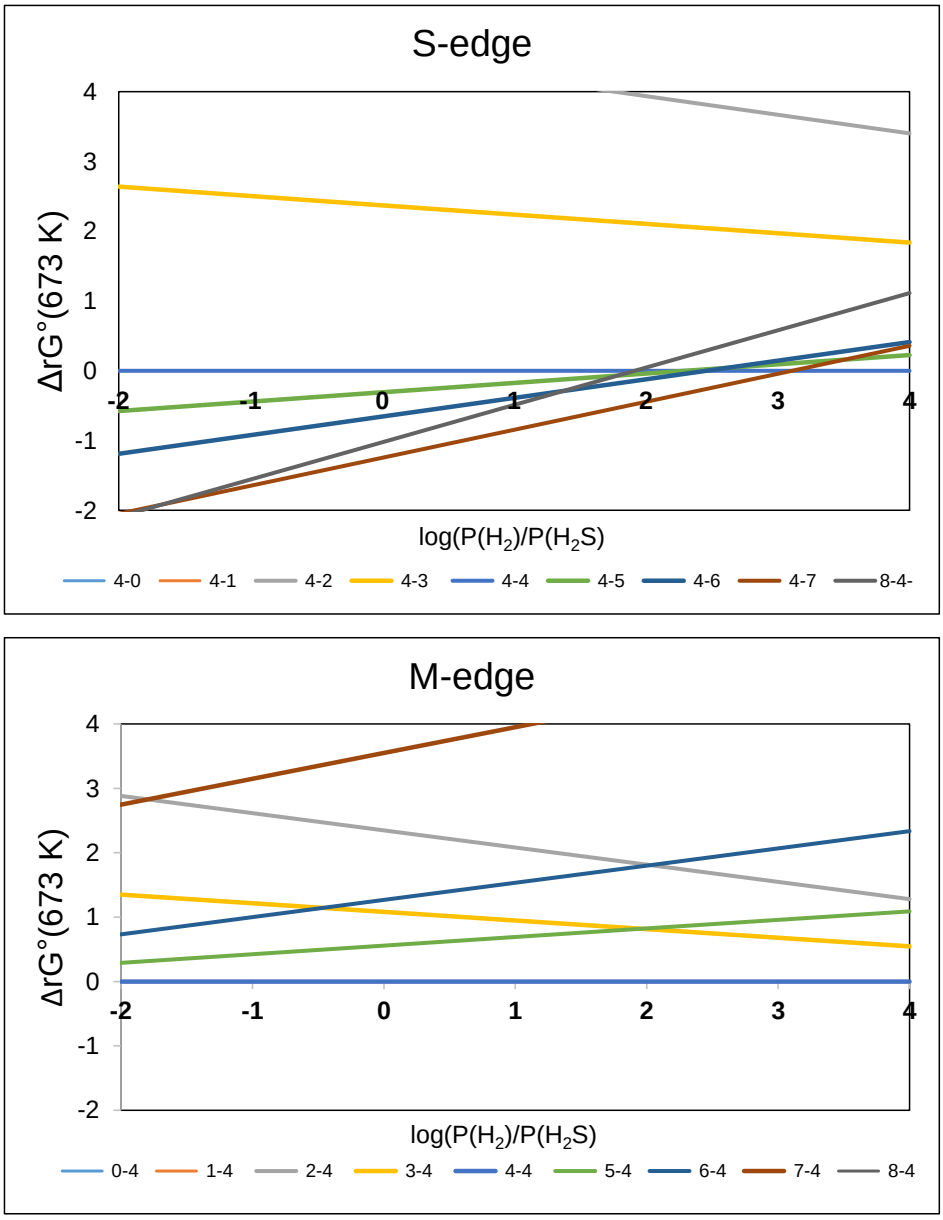

Figure 5. Free formation enthalpy (in eV) of the edges starting from the [4-4] surface at 673 K, as a function of $log\left(^{P_{H_2}}/_{P_{H_2S}}\right)$.

In sulfidation conditions, the most stable surface corresponds to [4 - 7] (**Figure 6**-A). The coordination of both the W atoms of the M-edge is six (VI) while on the sulfur edge, the coordination is five (V) for two W atoms and six (VI) for two W ones. Under this configuration, each W atom in the M-edge is bridged to 2 S atoms in the plane above the surface of the W atoms, while two W atoms in the S-edge are bridged to 4 S atoms in the plane above the surface of the W atoms and the two other ones bridges to only 3 S atoms. The second stable surface under reductive conditions is the [4 - 4] (**Figure 6**-B). The coordination numbers of W atoms are 6 on the M-edge (W_{6c}) and 4 (W_{4c}) on the S-edge. The terminal S atoms are in bridging position between two W atoms on both edges, the W-S distances are similar to the distances in the crystal (2.40 Å). Considering only coordination numbers, we can suppose that CO adsorption on the S-edge will be favored in a reductive environment. Here, the coordination of the W atoms of the S-edge decreases from V-VI to IV and the number of CUS increases when increasing the H_2/H_2S ratio, while no change was observed in the geometry of the M-edge.

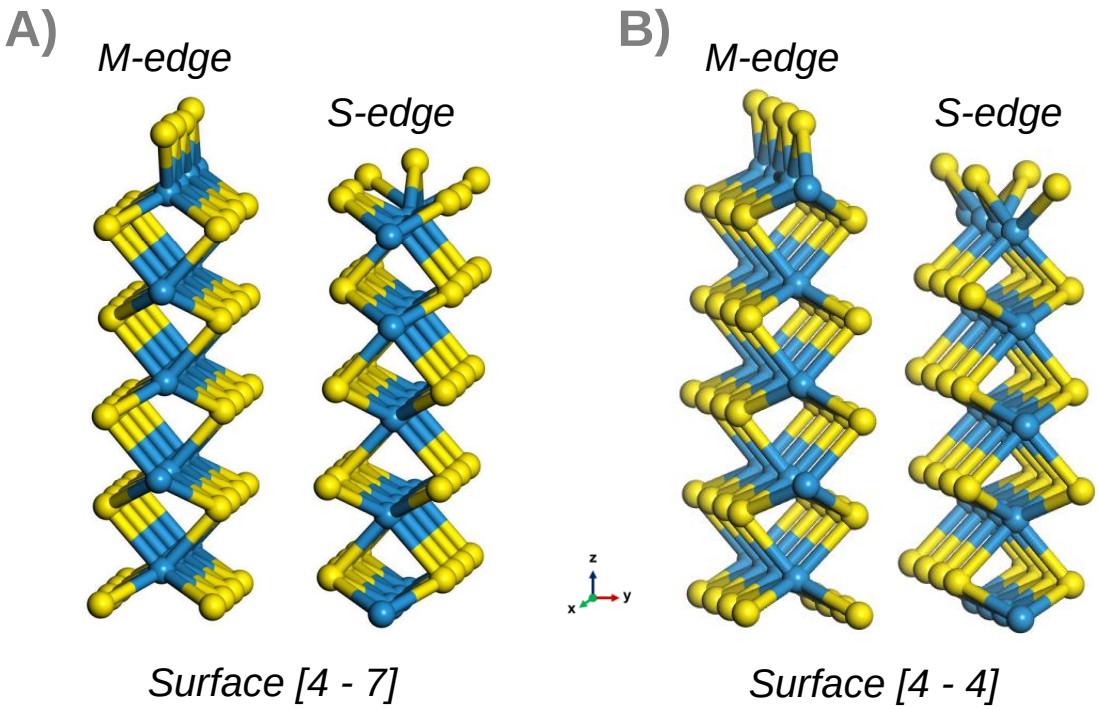

Figure 6. Depiction of the thermodynamic WS_2 stable surfaces according to the H_2S/H_2 partial pressures: (A) surface [4-7], stable surface when $H_2/H_2S < 500$; (B) surface [4 - 4], stable surface when $H_2/H_2S>500$.

3.2.2. Calculation of CO adsorption

The treatments to which the catalysts were subjected before the adsorption of CO were carried out to correspond to two of the three stable surfaces of the WS_2 edges. The stable zone corresponding to the sulfidation procedure under pure H_2S was not considered in our case since it is less frequently used at industrial level. All computed adsorption energies and vibrational frequencies of CO on [4 – 7] and [4 – 4] surfaces for both edges are reported in **Table I**.

Table I. Calculated parameters of CO adsorbed on M-edge (W) and S-edge (S) of WS_2.

Edge	Conditions	Surface	W coordination	E ads (eV)	v(CO) (cm^{-1})	D_{W-C} (Å)	D_{C-O} (Å)
M-	sulfidation	[4-x]	6	-0.63 to -0.70	2025	2.11	1.15
M-	reductive	[4-x]	6	-0.63 to -0.70	2025	2.11	1.15
S-	sulfidation	[x-7]	5	-0.40	1957	2.09	1.16
S-	reductive	[x-4]	4	-0.83 ; 1.04	1949 ; 1959	2.09	1.16

On the M-edge either in sulfiding or in reducing conditions [4 – x], CO adsorption can take place with an adsorption energy ranging between -0.63 to -0.70 eV, depending on the exact geometry of the M-edge. The geometry of the W surface is subject to Peierls distortion, but this does not lead to any effect on the ν(CO) frequency that is 2025 cm^{-1}.

Figure 7 represents the optimized geometry of the structure of the M-edge where the CO interacts with a single W atom. In **Figure 7-A** the optimized distances are depicted while in **Figure 7Figure 7-B** the coordination of the tungsten on the M-edge is shown.

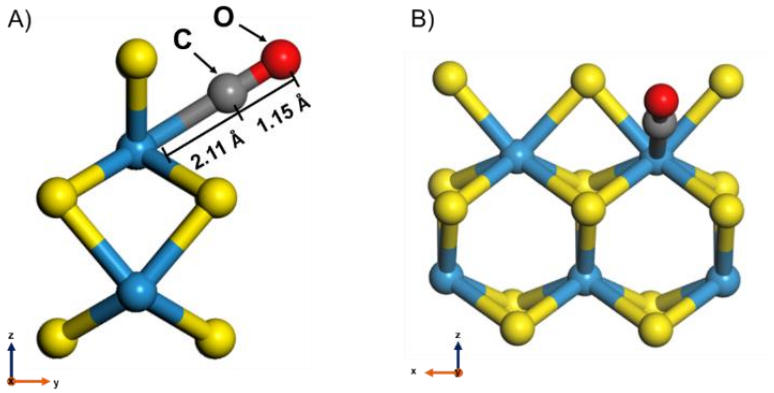

Figure 7. Optimized configuration for one CO molecule adsorbed on the M-edge [4-x] of WS_2 surface. A) Front view of the optimized distances between the W atom and the CO molecule. B) Side view of the M-edge showing the W coordination.

In sulfiding condition, the stable surface of the S-edge is [x – 7], a top CO adsorption on W_{5c} is also possible with adsorption energy of -0.40 eV. In this configuration, the CO molecule is almost perpendicular to the surface and the ν(CO) wavenumber is now calculated at 1957 cm^{-1}. In conditions corresponding to high hydrogen amount, the stable surface is the [x – 4]. The 3 S atoms are removed, creating 4 CUS sites (W_{4c} atoms) on the S-edge. The S atoms on the S-edge form a zigzag chain that is flexible. The sulfur atom can move from one side of the plan defined by the W atoms to the other side easily. On the most stable geometry, the adsorption energy is -1.04 eV and the associated wavenumber is 1959 cm^{-1}. The displacement of a sulfur atom form one side of the W plane to the other one reduced the stability of the S-edge, the adsorption energy is then -0.83 eV. In this configuration, the CO stretching wavenumber is computed at 1949 cm^{-1}. Thus there is a difference around 70 cm^{-1} between CO adsorbed on the S-edge and on the M-edge. Due to the multiple configurations of the S atoms on the S-edge, a broadening of the ν(CO) band on S-edge is expected.

A representation of the most stable structure is given in **Figure 8**. The CO molecule is adsorbed on the S-edge perpendicular to the surface (**Figure 8**-A).

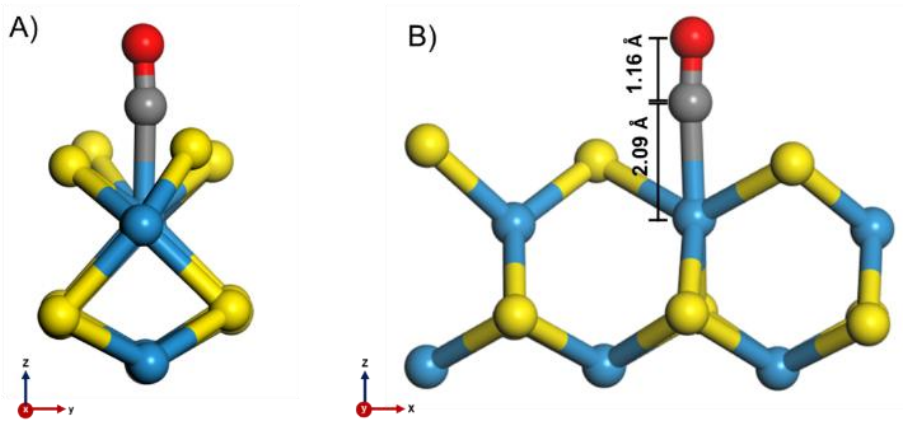

Figure 8. Optimized configuration for one CO molecule adsorbed on the S-edge [x-4] of WS_2 surface. A) Front view of the optimized distances between the W atom and the CO molecule. B) Side view of the S-edge showing the W coordination.

3.2.3. CO adsorption: Experiment vs Calculation

Experimental spectra present two main ν(CO) bands (W_1, W_2) separated by ~ 55 cm^{-1}. Their intensity ratio varies significantly with the conditions of treatment and preparation (**Figure 4** and **Figure 9**) indicating that they are characteristics of two distinct sites of the sulfided slabs. In parallel, DFT calculations show that CO adsorption on M-edge and on S-edge of WS_2 surface gives rise to ν(CO) bands separated by ~ 70 cm^{-1}. This allows us to propose assigning the high wavenumber band (W_1, 2121 cm^{-1}) to CO adsorbed on M-edge and the low wavenumber band (W_2, 2066 cm^{-1}) to CO adsorbed on S-edge. It should be mentioned that, as for DFT calculation, the differences of wavenumber are more reliable than the value of wavenumbers since no scaling factor nor anharmonic correction have been taken into account.

Other interesting parallels between experiment and calculation on W system appears. First, the experimental spectra (Figure 3 A and B) point out that the W_1 band

at 2121 cm^{-1} correspond to one single species and DFT calculation reports that there is one single geometry for CO adsorption on M-edge. Second, experiments show that the W_2 component comprised several bands (2075, 2066, 2051 cm^{-1}) and calculation shows for the CO adsorption on the S-edge that numerous geometries and orientations of the S atoms are stable, giving rise to more than one type of possible adsorption of CO at this edge. Moreover, despite the existence of different types of geometry, the variation of the calculated wavenumber from one band to another is relatively small (10 cm^{-1}).

Another feature to mention is that reductive treatment leads to almost no change of intensity of W_1 bands, while W_2 band increases slightly (**Figure 4**). This is in good agreement with trends reported by calculation that indicates no change in W coordination on M-edge and some changes in the W coordination on S-edge between sulfiding and reductive conditions (**Table I**) and also that the number of CUS site on the S-edge will increase in reducing conditions, while this number is constant on the M-edge.

The agreement between experimental and calculated features supports the assignment of the band at 2121 cm^{-1} to CO adsorption on M-edge ($CO_{M\text{-}edge}$) and that at ~2066 cm^{-1} to CO adsorption on S-edge ($CO_{S\text{-}edge}$).

3.3. Influence of W loading on W- and S-edge bands.

A series of W/Al_2O_3 catalysts, in which the W coverage was increased from 0.85 to 3.3 atoms·nm^{-2} (i.e. from 6 to 20 wt% W), has been analyzed by IR/CO from small CO doses up to 133 Pa at equilibrium. **Figure 9** compares the spectra obtained at 113 Pa

CO at equilibrium of the different W-catalysts, the inset shows the IR spectra obtained at sulfide site saturation.

As a general manner, bands similar as those reported on W_20/Al_2O_3 catalyst (**Figure 2**) are observed although with intensity and ratio that depends on the W amount and on the alumina coverage **Figure 9**. At the lowest metal loading (6 wt. %) and under 133 Pa of CO, v(CO) bands in the 2130-2000 cm^{-1} region are almost undetectable (**Figure 9**). This is partly due to the high intensity of the v(CO) bands associated with the support, which overshadow the signal corresponding to the sulfided sites. As the W concentration increases, the v(CO) bands associated to WS_2 sites gain intensity and are better defined (**Figure 9** – see insert). In addition to the well-visible band $CO_{M\text{-}edge}$ band, centered at 2121 cm^{-1}, the $CO_{S\text{-}edge}$ band begins to appear at 2066 cm^{-1}. The intensity of $CO_{S\text{-}edge}$ band increases with the W loading in the catalyst. On the other hand, the intensity of the v(CO) bands associated to the support (Al^{3+} Lewis acid sites and OH groups of Al_2O_3) decrease as a result of a more covered surface of the alumina support by WS_2, which agrees with the increase of the W loading.

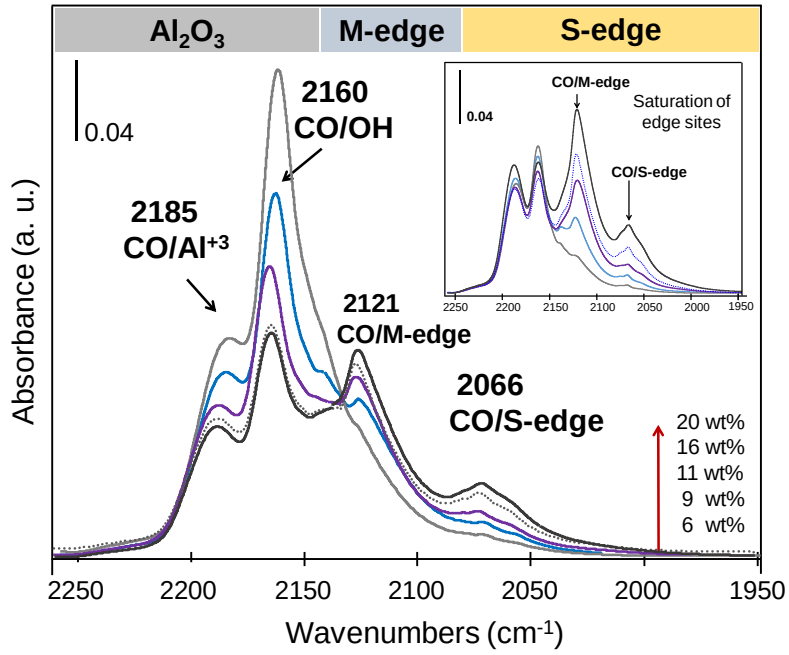

Figure 9. IR spectra of CO adsorption on WS_2/Al_2O_3 prepared with different W loading (Main: 133 Pa CO at equilibrium, Insert: at sulfide site saturation, both at 100 K). The WS_2/Al_2O_3 catalysts were obtained by sulfidation at 673 K and 0.1 MPa with 10% H_2S/H_2.

3.4. Determination of molar attenuation coefficients for W- and S-edge bands

In previous works of our group on MoS_2-based catalysts,[36] distinct molar attenuation coefficient values were obtained for CO adsorbed on either M-edge ($\mathcal{E}_{CO}$/M-edge) or S-edge ($\mathcal{E}_{CO}$/S-edge) (**Table II**). These values allowed the quantification of MoS_2 sites of each edges and thus calculation of the S-/M-edge ratio that defines the morphology of the MoS_2 slabs.[14] Recent work on sulfided Mo/Al_2O_3 catalysts prepared with and without citric acid showed a good agreement between sulfided slab shape determined from IR/CO, and that observed on transmission electron microscope by STEM-HAADF.[17] This gave a proof by image of the morphological changes of the catalyst according to the preparation modes, and also underlined that IR/CO method allows to reach a representative average picture of the sulfided slab shapes. Thus, the

determination of the morphology of the WS_2 particles requires the measurement of the molar attenuation coefficients of the v(CO) bands characteristics of M-edge and S-edge. In the literature, no ε_{CO} values for M-edge and S-edge are reported for any of the species formed in the WS_2 or NiWS catalysts. A close inspection of the spectra obtained for the first doses of CO introduced shows that, at low W loading, only one v(CO) band characteristic of M-edge sites appears (**Figure 10** A-C). However, spectra obtained on 6_W/Al_2O_3 present signals associated to CO adsorbed on alumina Lewis acid sites from the first CO doses. This is in agreement with the very limited support coverage by W phase (0.85 atoms·nm^{-2}), but this prevents using the spectra obtained on the catalyst with the lowest W amount to calculate $\varepsilon_{CO/M\text{-}edge}$ sites. However, when the W amount is somehow greater as for 9_W/Al_2O_3 and 12_W/Al_2O_3, the relationship between the variation of the band area of CO adsorbed on M-edge and the number of CO introduced can be used to calculate the $\varepsilon_{CO/M\text{-}edge.}$ As shown on **Figure 11**, close $\varepsilon_{CO/M\text{-}edge}$ values were obtained for these two catalysts i.e. 11.4 ± 2 cm·µmol^{-1} for 9_W/Al_2O_3 and 12.2 ± 2 cm·µmol^{-1} for 12_W/Al_2O_3. At higher W loading (**Figure 10** D-E) i.e. for 16_W/Al_2O_3 and 20_W/Al_2O_3, two v (CO) bands are detected even for low CO doses. They correspond to CO interaction with the M-edge site (2121 cm^{-1}) and the S-edge site (2072 cm^{-1}). With the molar attenuation coefficient of CO adsorbed on M-edge ($\varepsilon_{CO/M\text{-}edge}$) already determined, the amount of CO adsorbed specifically on M-edge sites can be calculated from the band area of these sites and using the methodology described in section 3.5. Hence, a relationship between the variation of the band area of CO adsorbed on S-edge and the number of CO adsorbed on S-edge sites (calculated from the total number of CO introduced in the cell minus the number of CO adsorbed on M-edge sites) was used

to calculate the attenuation coefficient of CO adsorbed on S-edge ($\varepsilon_{CO/S\text{-}edge}$). The slope of this relationship is the $\varepsilon_{CO/S\text{-}edge}$.

$$\left[\frac{n_T}{S} - \frac{A_{M-edge}}{\varepsilon_{M-edge}}\right] \varepsilon_{M-edge} = A_{S-edge} \qquad (3)$$

Note that a CO band specific of Lewis acid sites appears from the third CO doses, but the signal being low, it has been neglected in the $\varepsilon_{CO/M\text{-}edge}$ calculations. **Figure 11** shows that close $\varepsilon_{CO/S\text{-}edge}$ values are obtained for these two catalysts i.e. 22.9 ± 6 $cm \cdot \mu mol^{-1}$ for 16_W/Al_2O_3 and 23.4 ± 6 $cm \cdot \mu mol^{-1}$ for 20_W/Al_2O_3. Thus, the average molar attenuation coefficients $\varepsilon_{CO/M\text{-}edge}$ and $\varepsilon_{CO/S\text{-}edge}$ for sulfided W/Al_2O_3 catalysts are 11.9 ± 2 $cm \cdot \mu mol^{-1}$ and 23.1 ± 6 $cm \cdot \mu mol^{-1}$ respectively. Note that in all the calculations (**Figure 11**) an adequate fit and line tendency were obtained.

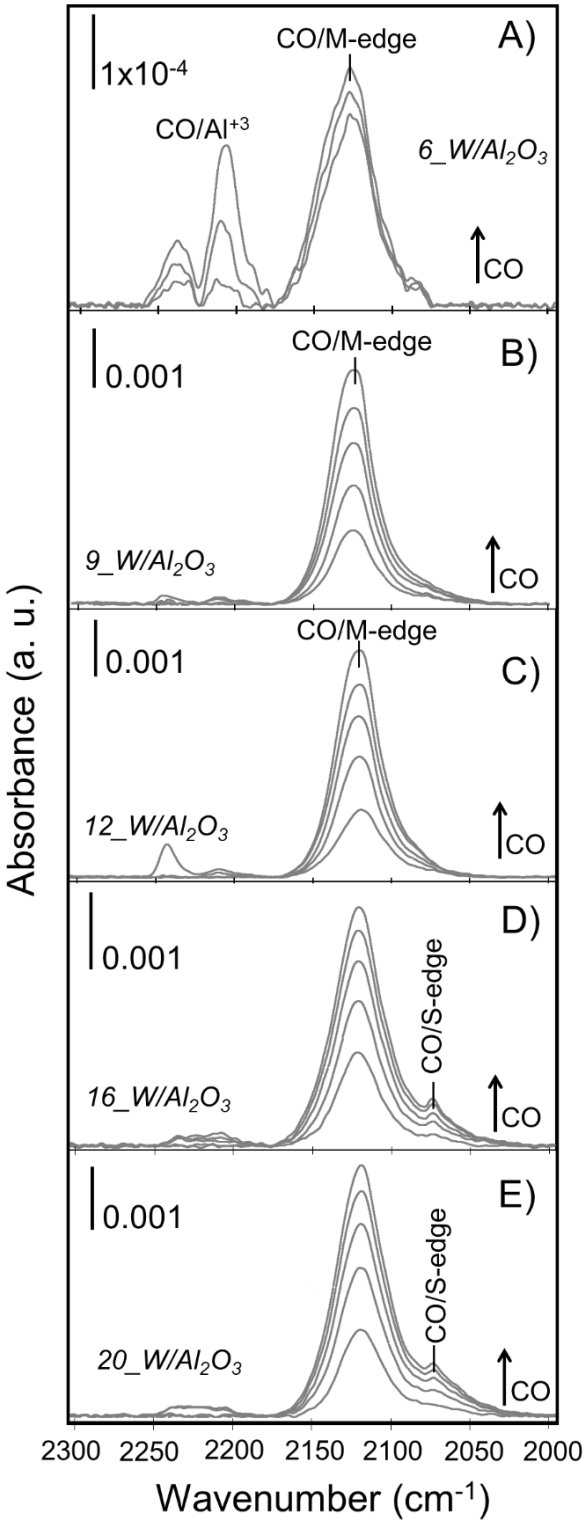

Figure 10. IR spectra of the first CO doses adsorbed (T = 100 K) on sulfided W/Al_2O_3 at different metal loadings. Intermediate W concentrations results on CO adsorption only on the metallic edge. (first doses: 0.001, 0.002, 0.003, and 0.004 μmol $CO \cdot mg^{-1}$ sulfided catalyst).

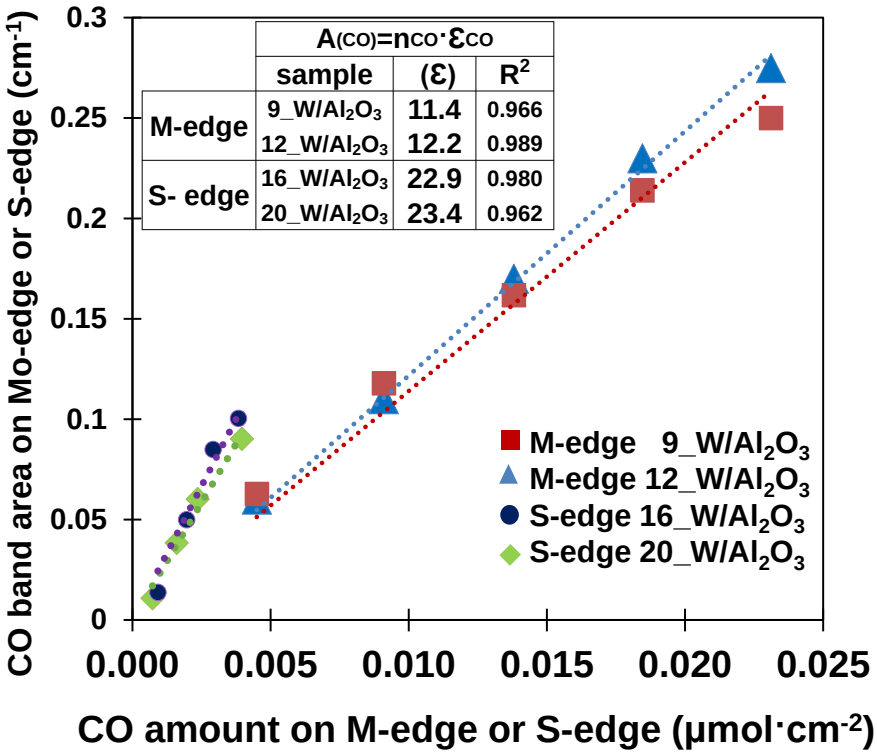

Figure 11. Determination of the molar attenuation coefficients (Ɛ) of CO adsorbed on WS_2. The spectra for Ɛ determination are reported in **Figure 9**. The Ɛ values are the slope of the linear relationship between the area of ν(CO) band and the amount of CO introduced onto a cm^2 of the sample.

3.5. The influence of W loading on WS_2 slab morphology.

As observed in **Figure 9**, the increase of metal loading has an effect not only on the intensity of the bands associated to the M- and S- edges, but also on their ratio. From the molar attenuation coefficients for both edge sites, the S-edge/M-edge ratio can be calculated for the various W catalysts (**Figure 12**). The value of the ratio undergoes a steady increase along with the W loading and shows that the morphology of the WS_2 slabs changes from slightly truncated triangles exposing mainly the M-edge (S-edge/M-edge = 0.17) to a more heavily truncated triangle exposing more S-edge (S-edge/M-

edge = 0.32). Similar effect of metal loading has been earlier reported for MoS_2/Al_2O_3 catalysts.[13] In Mo system, this phenomenon was associated to a change in the sulfide phase - support interactions with metal loading. This, since the MS_2 phase interacts with Al_2O_3 support by the M–O–Al linkages that are located at the edges of the slabs instead of at the core slab sites.[13,37] Similarly, the concentration of the W–O–Al linkages will decreases with increasing WS_2 size. It is observed that the WS_2 slabs on WS_2/Al_2O_3 catalysts exposed more S-edge with increasing the W loading. All these results suggest that the WS_2–Al_2O_3 interactions decrease with increasing W loading.

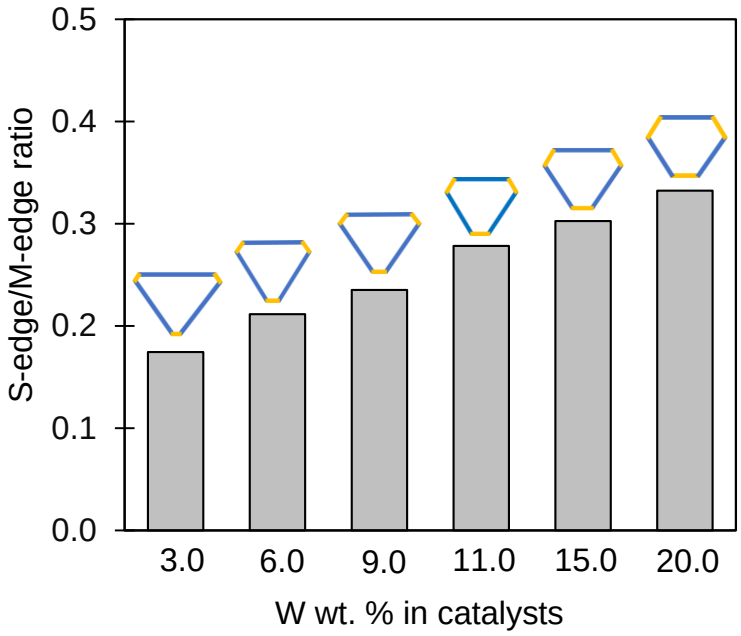

Figure 12. The ratios of S-edge/M-edge and corresponding morphologies of WS_2 slabs as function of W loading of WS_2/Al_2O_3 catalysts.

3.6. Comparison between W and Mo sulfide catalysts.

As summarized in **Table II**, many similarities appear for CO adsorption on W and Mo sulfide catalysts.

For sulfide W as well as for sulfide Mo catalysts, CO adsorbed on sulfide slabs gives rise to 2 IR bands separated by about 50 cm^{-1} that allows distinguishing M-edge ($CO_{M\text{-}edge}$) and S-edge ($CO_{S\text{-}edge}$). On both systems, the frequencies of $CO_{M\text{-}edge}$ appear at greater frequency than the $CO_{S\text{-}edge}$. This is in agreement with the calculated Mo and W coordination that is greater on M-edge (M_{6C}) than on S-edge (M_{4C}) (Table 1, Ref. [10]). In agreement with their higher frequencies, molar attenuation coefficient (Ɛ) for $CO_{M\text{-}edge}$ is greater than for $CO_{S\text{-}edge}$. From these values, the morphology of the TMS slabs could be calculated. For alumina supported catalysts with metal amount corresponding to monolayer coverage, sulfided slabs with very close morphology i.e. highly truncated triangle (S-/M- ratio = 0.30-0.32) are formed on alumina supported Mo and W catalysts.

In both systems, an accurate analysis shows that CO adsorbed on S-edge is characterized by a broad band consisting of several ν(CO) components. The three bands (2065, 2045 and 2020 cm^{-1}) characterizing CO adsorption on S-edge of Mo/Al_2O_3 have been associated to different CO coverages.[10,11,36,38] Whereas the three components (2075, 2066 and 2051 cm^{-1}) detected on S-edge of W/Al_2O_3 have been associated to various orientations of the edge sulfur atoms giving rise to more than one ν(CO) band. It must be noted that the relatively small model used to describe the MoS_2 S edge, does not allows various geometries. By contrast, M-edge sites present a more homogeneous geometry. For W catalyst, only one component is detected whatever the H_2S/H_2 ratio whereas for Mo/Al_2O_3 system, a band is detected at 2110 cm^{-1} after sulfidation while a second one develops under reductive atmosphere (2098 cm^{-1}).[10,36]

A noticeable difference between the Mo and W systems is their difference of stability toward reductive treatment. When submitted to H_2-post-treatment, the stability

of the edge sites of sulfide W catalyst is remarkable (only S-edge site amount increases by 16%). By contrast, on Mo system, the CO uptake increases of about 55% both on M- and S-edges. This great sulfur depletion of MoS_2 edge is in agreement with the appearance of a new band (2098 cm^{-1}) after reductive treatment whereas no frequency shift are observed on W catalysts.

Hence, sulfided slabs of Mo and W alumina supported catalysts present similar morphologies but different stability regarding H_2 treatment.

Table II. Comparison of experimental ν(CO) frequencies and molar attenuation coefficients of CO on M- and S-edge, as well as MS_2 slab morphology for (9 %) Mo/Al_2O_3 and (20 %) W/Al_2O_3 catalysts sulfided under H_2S/H_2* or post –treated under H_2 at 473K atmosphere.

		Sulfidation		H_2 post-treatment vs sulfidation
Catalyst	Edge type	ν(CO) frequency (cm^{-1})	Epsilon, ε_{CO} ($cm \cdot \mu mol^{-1}$)	CO band area enhancement
Mo	M-edge	2110	20.0 ± 3	+60%
	S-edge	2065	35.0 ± 9	+54%
	Slab morphology	Truncated triangle Ratio S/M = 0.30		
W	M-edge	2121	11.9 ± 2	~0%
	S-edge	2066	23.1 ± 6	+16%
	Slab morphology	Truncated triangle Ratio S/M = 0.32		

* Values corresponding to a metal close to monolayer (at the oxidic state) on the alumina surface.
Sulfidation conditions: Mo/Al_2O_3 Ts = 423 K, 2h : W/Al_2O_3 Ts = 473 K, 2h.

4. CONCLUSIONS

In the present work, carbon monoxide adsorption on alumina-supported sulfided W catalysts was studied by means of IR spectroscopy pairing with DFT calculations. The parallel between experimental and calculated data allowed us to attribute, for the first time, the two v(CO) bands observed at 2121 cm^{-1} and about 2066 cm^{-1} to CO adsorbed on the M-edge and S-edge sites of the WS_2 slabs, respectively.

The integrated molar attenuation coefficients of CO associated with the M- and S-edge sites were determined, allowing determination of the WS_2 morphology. Increasing the W loading (3-20 wt% W) allows going from an almost pure triangle exhibiting mostly M-edge to a truncated triangle.

Parallel between experiments and DFT calculation of CO adsorption on W and Mo sulfide catalysts provides evidence for many similarities between the two systems. On both TMS, CO adsorption give rise to two main ν (CO) bands separated by about 50 cm^{-1} that allowed to discriminate M-edge and S-edge sites. For M loading close to monolayer coverage of alumina (in oxidic form), Mo and W sulfide slab present a similar shape i.e. truncated triangle. However, edge sites of WS_2 slabs clearly exhibit greater stability under H_2 atmosphere than Mo sulfided ones.

Acknowledgements

L. Zavala-Sanchez acknowledges the Mexican National Council for Science and Technology (CONACYT) for the Ph. D. grant. The authors acknowledge LABEX EMC3

from ANR for the financial support to MIMOSA project. DFT calculations have been performed on the Lille University Calculation center partially funded by Feder.

REFERENCES

[1] T. Kabe, A. Ishihara, Q. Zhang, *Appl. Catal. A Gen.* **1993**, *97*, L1–L9.

[2] C. E. Santolalla-Vargas, V. A. Suarez Toriello, J. A. De los Reyes, D. K. Cromwell, B. Pawelec, J. L. G. Fierro, *Mater. Chem. Phys.* **2015**, *166*, 105–115.

[3] V. A. Suárez-Toriello, C. E. Santolalla-Vargas, J. A. De Los Reyes, A. Vázquez-Zavala, M. Vrinat, C. Geantet, *J. Mol. Catal. A: Chem.* **2015**, *404–405*, 36–46.

[4] M. Brorson, A. Carlsson, H. Topsøe, *Catal. Today* **2007**, *123*, 31–36.

[5] F. E. Topsøe, H., Clausen, B. S., & Massoth, *Catalysis Science and Technology*, Springer, Berlin, **1996**.

[6] Y. Okamoto, K. Hioka, K. Arakawa, T. Fujikawa, T. Ebihara, T. Kubota, *J. Catal.* **2009**, *268*, 49–59.

[7] J. Chen, F. Maugé, J. El Fallah, L. Oliviero, *J. Catal.* **2014**, *320*, 170–179.

[8] I. Khalil, H. Jabraoui, G. Maurin, S. Lebègue, M. Badawi, K. Thomas, F. Maugé, *J. Phys. Chem. C* **2018**, *122*, 26419–26429.

[9] H. Jabraoui, I. Khalil, S. Lebègue, M. Badawi, *Mol. Syst. Des. Eng.* **2019**, *4*, 882–892.

[10] A. Travert, C. Dujardin, F. Maugé, S. Cristol, J. F. Paul, E. Payen, D. Bougeard, *Catal. Today* **2001**, *70*, 255–269.

[11] A. Travert, C. Dujardin, F. Maugé, E. Veilly, S. Cristol, J.-F. Paul, E. Payen, *Phys. Chem. B* **2006**, *110*, 1261–1270.

[12] F. Maugé, J. C. Lavalley, *J. Catal.* **1992**, *137*, 69–76.

[13] J. Chen, L. Oliviero, X. Portier, F. Maugé, *RSC Adv.* **2015**, *5*, 81038–81044.

[14] J. Chen, E. Dominguez Garcia, E. Oliviero, L. Oliviero, F. Maugé, *J. Catal.* **2016**, *339*, 153–162.

[15] E. Dominguez Garcia, J. Chen, E. Oliviero, L. Oliviero, F. Maugé, **2020**.

[16] M. Vrinat, M. Breysse, C. Geantet, J. Ramirez, F. Massoth, *Catal. Letters* **1994**, *26*, 25–35.

[17] L. Zavala-sanchez, X. Portier, F. Maugé, L. Oliviero, *Nanotechnology* **2019**, 1–10.

[18] E. J. M. Hensen, Y. Van Der Meer, J. A. R. Van Veen, J. W. Niemantsverdriet, *Appl. Catal. A Gen.* **2007**, *322*, 16–32.

[19] T. Alphazan, A. Bonduelle-Skrzypczak, C. Legens, A. S. Gay, Z. Boudene, M. Girleanu, O. Ersen, C. Copéret, P. Raybaud, *ACS Catal.* **2014**, *4*, 4320–4331.

[20] J. Chen, E. Dominguez Garcia, L. Oliviero, F. Maugé, *J. Catal.* **2015**, *332*, 77–82.

[21] J. Hafner, *J. Comput. Chem.* **2008**, *29*, 2044–2078.

[22] G. Kresse, J. Furthmiiller, *Comput. Mater. Sci.* **1996**, *6*, 15–50.

[23] J. P. Perdew, *Phys. Rev. B* **1986**, *33*, 8822–8824.

[24] J. P. Perdew, K. Burke, M. Ernzerhof, *Phys. Rev. Lett.* **1996**, *77*, 3865–3868.

[25] G. Kresse, D. Joubert, *Phys. Rev. B Condens. matter Mater. Phys.* **1999**, *59*, 1758–1775.

[26] J. D. Pack, H. J. Monkhorst, *Phys. Rev. B Condens. matter Mater. Phys.* **1977**, *16*, 1748.

[27] H. Hijazi, L. Cantrel, J.-F. O. Paul, *J. Phys. Chem. C* **2018**, *122*, 26401–26408.

[28] H. J. Monkhorst, J. D. Pack, *Phys. Rev. B* **1976**, *13*, 5188–5192.

[29] S. Cristol, J. F. Paul, E. Payen, D. Bougeard, S. Clémendot, F. Hutschka, *Phys. Chem. B* **2000**, *104*, 11220–11229.

[30] D. Duchet, J. C., Lavalley, J. C., Housni, S., Ouafi, D., Bachelier, J., Lakhdar, M., ... & Cornet, *Catal. Today* **1988**, *4*, 71–96.

[31] B. Muller, A. D. Van Langeveld, J. A. Moulijn, H. Knozinger, *J. Phys. Chem* **1993**, *97*, 9028–9033.

[32] J. P. Ouafi, Driss, Mauge, Francoise, Bonelle, *Catal. Today* **1988**, 23–37.

[33] G. Crepéau, Caracterisation de l'acidite de Catalyseurs d'hydrocraquage Amorphes Sulfures., University of Caen, **2002**.

[34] A. Travert, H. Nakamura, R. A. Van Santen, S. Cristol, J.-F. O. Paul, E. Payen, **2002**.

[35] S. Cristol, J. F. Paul, E. Payen, D. Bougeard, S. Clémendot, F. Hutschka, **2002**.

[36] J. Chen, V. Labruyere, F. Maugé, A. A. Quoineaud, A. Hugon, L. Oliviero, *J. Phys. Chem. C* **2014**, *118*, 30039–30044.

[37] D. Costa, C. Arrouvel, M. Breysse, H. Toulhoat, P. Raybaud, *J. Catal.* **2007**, *246*,

325–343.

[38] C. Dujardin, M. A. Lélias, J. Van Gestel, A. Travert, J. C. Duchet, F. Maugé, **2007**.

Entry for the Table of Contents

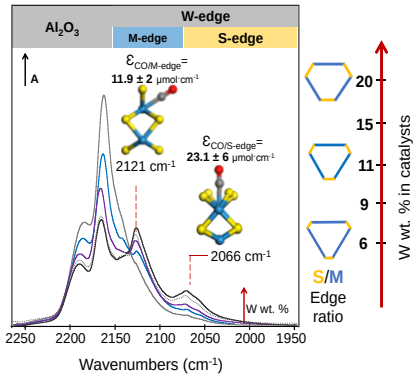

Text for Table of Contents:

CO adsorption on sulfided W/Al_2O_3 catalysts was studied by IR spectroscopy pairing with DFT calculations. Parallel between experimental and calculated data allowed to attribute, for the first time, the two v(CO) bands observed at 2121 cm^{-1} and ~2066 cm^{-1} to CO adsorbed on the M-edge and S-edge sites respectively. The molar attenuation coefficients for CO adsorbed at the M-edge and the S-edge were determined. This allowed the morphology of the WS_2 slabs to be calculated.